Solution-Processable Red-Emission Organic Materials Containing Triphenylamine and Benzothiodiazole Units: Synthesis and Applications in Organic Light-Emitting Diodes

ARTICLE *in* THE JOURNAL OF PHYSICAL CHEMISTRY B · JULY 2009

Impact Factor: 3.3 · DOI: 10.1021/jp900362f · Source: PubMed

7 AUTHORS, INCLUDING:

Yi Zhou
Soochow University (PRC)
48 PUBLICATIONS **1,695** CITATIONS
SEE PROFILE

Qingguo HE
Shanghai Institute of Microsystem And Info…
76 PUBLICATIONS **1,129** CITATIONS
SEE PROFILE

Chang He
Chinese Academy of Sciences
50 PUBLICATIONS **2,050** CITATIONS
SEE PROFILE

F. Bai
Chinese Academy of Sciences
131 PUBLICATIONS **1,881** CITATIONS
SEE PROFILE

Solution-Processable Red-Emission Organic Materials Containing Triphenylamine and Benzothiodiazole Units: Synthesis and Applications in Organic Light-Emitting Diodes

Yi Yang,[†,‡] Yi Zhou,[†,‡] Qingguo He,[*,§] Chang He,[†,‡] Chunhe Yang,[†,‡] Fenglian Bai,[*,†] and Yongfang Li[*,†]

Beijing National Laboratory for Molecular Sciences, CAS Key Laboratory of Organic Solids, Institute of Chemistry, Chinese Academy of Sciences, Beijing, 100190, People's Republic of China, Graduate University of the Chinese Academy of Sciences, Beijing, 100039, People's Republic of China, and Shanghai Institute of Microsystem and Information Technology, Chinese Academy of Sciences, Shanghai 200050, China

Received: January 13, 2009; Revised Manuscript Received: April 10, 2009

Three solution-processable red-emissive organic materials with a hole-transporting unit triphenylamine (TPA) as the core part and a D−π−A bipolar structure as the branch part, TPA-BT (single-branched molecule), b-TPA-BT (bibranched molecule), and t-TPA-BT (tribranched molecule), were synthesized by the Heck coupling reaction. Herein, for the D−π−A push−pull structure, we use TPA as the electron donor, benzothiodiazole (BT) as the electron acceptor, and the vinylene bond as the π-bridge connecting the TPA and BT units. The compounds exhibit good solubility in common organic solvents, benefited from the three-dimensional spatial configuration of TPA units and the branch structure of the molecules. TPA-BT, b-TPA-BT, and t-TPA-BT show excellent photoluminescent properties with maximum emission peaks at ca. 630 nm. High-performance red-emission organic light-emitting diodes (OLEDs) were fabricated with the active layer spin coated from a solution of these compounds. The OLED based on TPA-BT displayed a low turn-on voltage of 2.0 V, a maximum luminance of 12192 cd/m^2, and a maximum current efficiency of 1.66 cd/A, which is among the highest values for the solution-processed red-emission OLEDs. In addition, high-performance white-light-emitting diodes (WLEDs) with maximum luminance around 4400 cd/m^2 and maximum current efficiencies above 4.5 cd/A were realized by separately doping the three TPA-BT-containing molecules as red emitter and poly(6,6′-bi-(9,9′-dihexylfluorene)- co-(9,9′-dihexylfluorene-3-thiophene-5′-yl)) as green emitter into blue poly(9,9-dioctylfluorene-2,7-diyl) host material with suitable weight ratios.

1. Introduction

Organic light-emitting diodes (OLEDs) based on either small molecules or polymers have been drawing broad attention due to their potential applications in full-color, flat-panel displays and lighting since Tang's[1] and Burroughes'[2] pioneering works.[3,4] Many new materials with RGB (red, green, blue) emission have been developed to meet the requirement of full-color displays.[5] Compared with green and blue, the development of red-light-emitting materials is far behind in terms of both purity and efficiency.[6−9]

Conventional red-emitting organic materials are the molecules either bearing a strong donor−acceptor polar substituent, such as pyran-containing dyes,[10−14] or with extended π conjugation, such as porphyrin-type macrocyclic compounds.[15−17] These materials tend to aggregate in highly concentrated solutions and solid states because of $\pi-\pi$ interaction or strong charge-transfer character and cannot form uniform thin films. Also, the aggregation could result in concentration quenching.[18] Thereby, they are commonly used as dopants in device fabrication to realize high-luminance OLEDs. However, OLEDs based on dopant emitters are more difficult to adapt for mass production processes, considering the reproducibility of the optimum doping level that requires careful manufacture control. Realistically, red-emissive materials with weak intermolecular interaction and good solubility which could be used by spin coating other than vacuum deposition is highly required for low-cost OLED fabrication.[19]

Here we report three red-emission and solution-processable amorphous molecular materials, TPA-BT, b-TPA-BT (bi-branched molecule), and t-TPA-BT (tribranched molecule) (see Figure 1). Yasuhiko Shirota's group[20−23] has done much fundamental study about the bipolar structure and amorphous molecular materials. They suggested that the bipolar radical formant character could allow both stable cation and anion radicals and balance the hole and electron carriers. We choose benzothiodiazole (BT) and triphenylamine (TPA) as the two basic moieties in the molecules in consideration of their high electron- and hole-transporting mobility.[24−31] Also, the vinylene bond was employed as a linkage to connect TPA and BT for constructing the conjugated push−pull branch unit (D−π−A) to realize red emission via strong intramolecular charge transfer. This bipolar branch structure bearing both electron-donating and electron-accepting moieties is capable of balancing charge carrier injection and can improve the charge recombination efficiency. The combination of the nonplanar TPA core with a linear π-conjugated branch could lead to amorphous conjugated materials with good solution processability[24,32−35] for decreasing the intermolecular $\pi-\pi$ stacking and reducing luminance quenching by aggregation.

These three molecules exhibited good solubility (concentrations of the three compounds in CB or toluene are over 18 mg/

* To whom correspondence should be addressed. (Y.Li) E-mail: liyf@iccas.ac.cn. Fax: 86-10-62559373. (Q.He) E-mail: hqg@mail.sim.ac.cn. Fax: 86-21-62511070-8934.

† Institute of Chemistry, Chinese Academy of Sciences.

‡ Graduate University of the Chinese Academy of Sciences.

§ Shanghai Institute of Microsystem and Information Technology, Chinese Academy of Sciences.

10.1021/jp900362f CCC: $40.75
Published on Web 05/11/2009

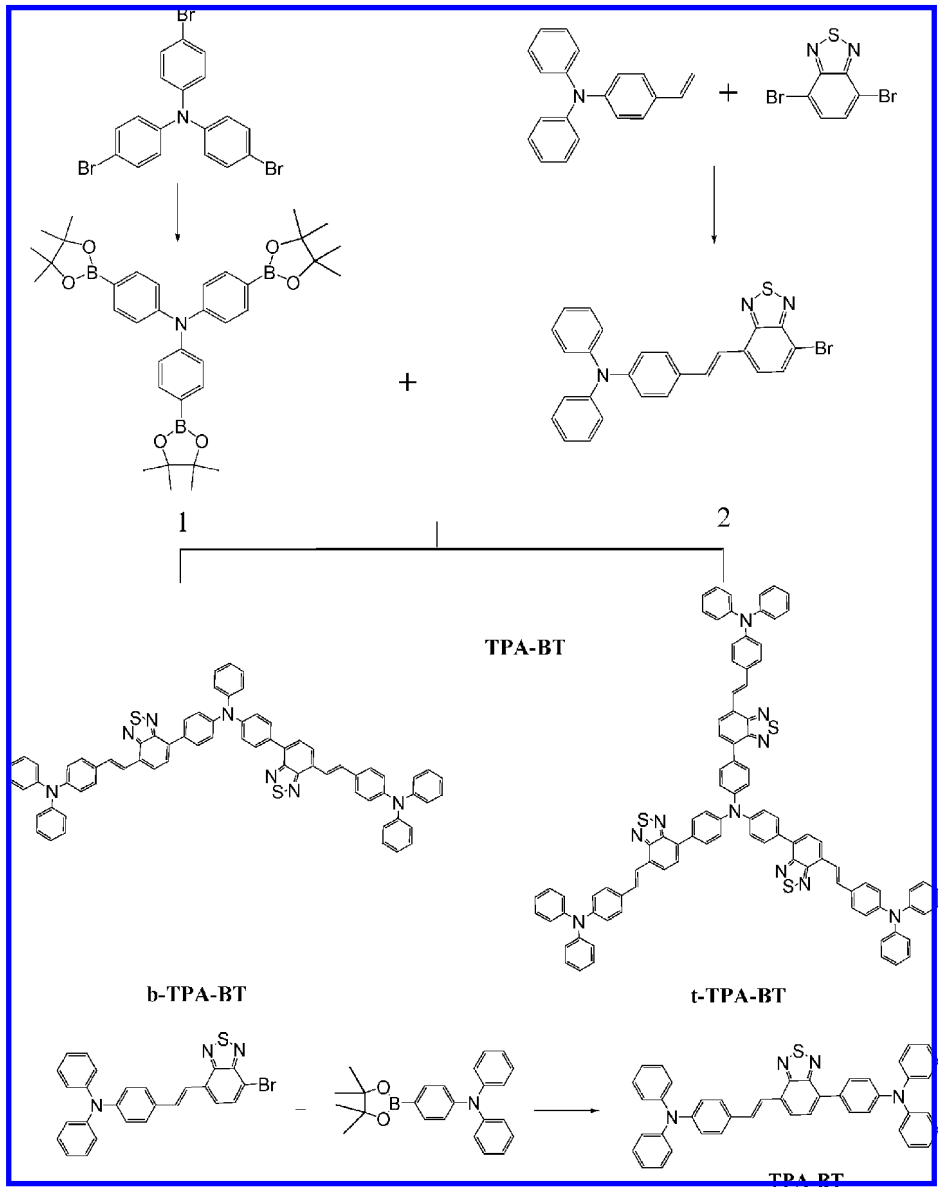

Figure 1. Synthetic routes and chemical structures of compounds TPA-BT, b-TPA-BT, and t-TPA-BT.

mL) and high thermal properties, which make them possible to be used in fabricating OLED devices by the spin-coating process. The OLEDs with TPA-BT as the emissive layer showed red emission with a maximum luminance of ca. 12,200 cd/m^2 and EL current efficiency of 1.66 cd/A, which is among the highest value for the solution-processed red-emission OLEDs.[36,37] Furthermore, by using these molecules as red emitters, high-performance white-light-emitting diodes (WLEDs) were achieved with a maximum luminance around 4400 cd/m^2 and maximum luminescence efficiency above 4.5 cd/A.

2. Results and Discussion

2.1. Synthesis. The synthetic routes of the three TPA-containing compounds are outlined in Figure 1. Synthesis of compound TPA-BT was conducted by reaction of TPA-monoborate and compound **2** with a high yield of 96% as shown in Figure 1. b-TPA-BT and t-TPA-BT were obtained via reaction of compounds **1** (triphenylamine triboronic acid tripinacol ester) and **2** in one pot. b-TPA-BT was obtained as a side product formed by the reaction of compound **2** and the diboronic acid dipinacol ester, which could be produced by the decomposition of triboronic acid tripinacol ester under the base condition. All molecular structures were verified by ^{1}H MNR, ^{13}C NMR, and MALDI-TPF-MS (see Experimental Section).

2.2. Photophysical Properties. Figure 2 displays the absorption and photoluminescence (PL) spectra of TPA-BT, b-TPA-BT, and t-TPA-BT dilute solutions in chloroform and solid films on a quartz substrate at room temperature. It can be seen from Figure 2a that there are two groups of absorption bands between 300 and 600 nm for the molecules solutions. The UV absorption bands peaked at ca. 315−328 nm can be assigned to $\pi-\pi^*$ transitions.[26] Also, the visible absorption peaks located around 490−500 nm resulted from an intramolecular charge transfer (ICT) from the donor (TPA) to the acceptor (BT).[38] The visible absorption peaks red shift and are enhanced from the linear (single branch) molecule TPA-BT to bibranched molecule b-TPA-BT to tribranched molecule t-TPA-BT. This phenomenon could be ascribed to a more expanded conjugation length and the electron coupling effect with the increased number of branches. Differing from their absorption spectra, the PL spectra of the three molecules solutions are nearly the same (also in Figure 2a), peaked at 651 nm, which suggests that the emission

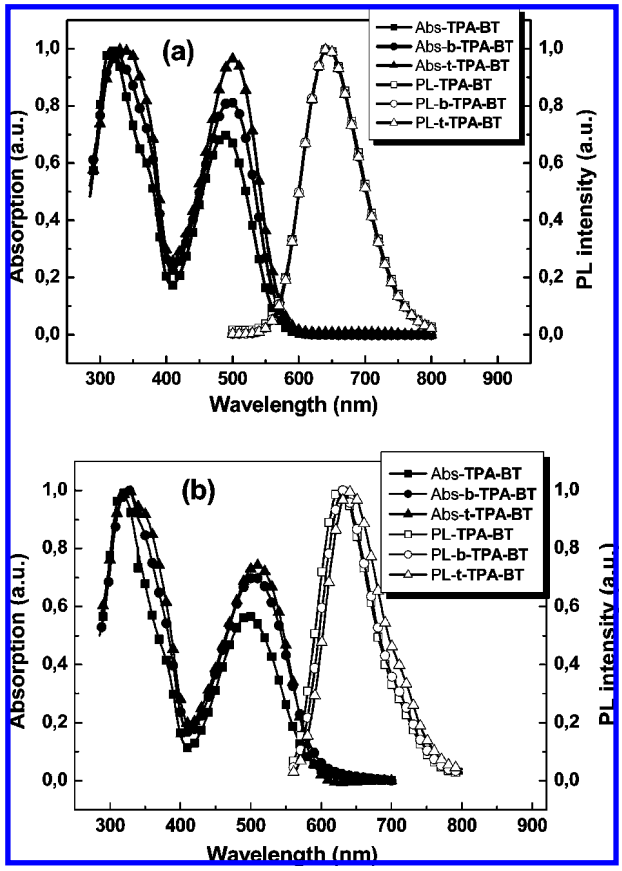

Figure 2. Absorption and PL spectra of TPA-BT, b-TPA-BT, and t-TPA-BT solutions in chloroform (a) and thin solid films (b).

band could come from the same intramolecular charge transfer state of TPA and BT units in the molecules.

The absorption spectra of the molecules films, as shown in Figure 2b, are slightly red shifted by 6−8 nm compared to that of the solutions, which implies a weak intermolecular interaction in the solid state. On the basis of the absorption edges of the TPA-BT (597 nm), b-TPA-BT (602 nm), and t-TPA-BT (605 nm) films, the corresponding optical energy bandgaps (E_g^{opt}) are calculated as 2.07, 2.06, and 2.05 eV, respectively. All their films showed red emission with a λ_{max} above 620 nm, blue shifted by about 10−15 nm compared to that of the solutions.

The fluorescence quantum yields of the molecules solutions in toluene were determined to be 47%, 54%, and 54% for TPA-BT, b-TPA-BT, and t-TPA-BT, respectively, with DCM as the standard; the measurement method is according to our previous publication.[39] As listed in Table 1, these values are high enough to be used as candidate emitters for OLEDs.

2.3. Electrochemical Properties. Electrochemical properties of the materials were investigated by cyclic voltammetry (CV), and samples were coated on the surface of the Pt working electrode by a solution-casting process. The cyclic voltammograms of TPA-BT, b-TPA-BT, and t-TPA-BT are shown in Figure 3. All three compounds exhibit reversible oxidation processes, indicating their high electrochemical stability for p-doping. The oxidation peak positions of TPA-BT and b-TPA-BT are nearly the same, while that of t-TPA-BT is a little widened and positively shifted. The reduction potential falls in a similar range to other BT-based small molecules.[40−43] The reduction potential is slightly lowered when the number of branches is increased (from TPA-BT to b-TPA-BT to t-TPA-BT).

The onset oxidation (E_{ox}^{onset}) and reduction potentials (E_{red}^{onset}) of the materials were 0.43 and −1.63 V for TPA-BT, 0.36 and −1.68 V for b-TPA-BT, and 0.44 and −1.72 V for t-TPA-BT, respectively, relative to the Ag/Ag^+ electrode. From the values of E_{ox}^{onset} and E_{red}^{onset}, the highest occupied molecular orbital (HOMO) and the lowest unoccupied molecular orbital (LUMO) as well as the electrochemical band gaps (E_g^{CV}) of the compounds were calculated according to the equations below.[44]

$$\text{HOMO} = -e(E_{ox}^{onset} + 4.71)\ (\text{eV}) \quad (1)$$

$$\text{LUMO} = -e(E_{red}^{onset} + 4.71)\ (\text{eV}) \quad (2)$$

$$E_g^{CV} = -e(E_{ox}^{onset} + E_{red}^{onset})\ (\text{eV}) \quad (3)$$

The electrochemical data are listed in Table 2. The HOMO and LUMO energy levels determined from the oxidation and reduction potential are in agreement with those estimated from the edges of the electronic absorption bands.

2.4. Red-Emission OLEDs. The OLEDs with TPA-BT, b-TPA-BT, or t-TPA-BT as the emissive layer were fabricated by the spin-coating process for investigating the electroluminescent (EL) properties of the compounds. The structure of the devices was ITO/PEDOT:PSS(30 nm)/PVK:poly-TPD(40 nm)/EML(60 nm)/Ca(10 nm)/Al(100 nm), where the blend of PVK:poly-TPD (1:1, wt/wt) was used as the hole-transporting layer (HTL) and the EML (emitting layer) was composed of TPA-BT, b-TPA-BT, or t-TPA-BT. For the convenience of discussion, the three OLED devices were named device A, device B, and device C for the OLEDs based on TPA-BT, b-TPA-BT, and t-TPA-BT, respectively. A binary hole-transporting layer, which was composed of the blend of two hole-transporting materials PVK and poly-TPD, was chosen in the devices as reported by Sun et al.[39,45−47] Poly-TPD in the HTL can resist the solvent dissolving during the spin coating of the EML and form a smooth interface between the two layers. In addition, considering the energy levels (shown in Figure 4) of materials used in the OLEDs, PVK with a higher LUMO level can play a role as an electron-blocking material in the HTL. Therefore, the binary HTL combines the advantages of both poly-TPD and PVK.

The electroluminescence (EL) spectra of devices A−C shown in Figure 5 were nearly identical with the PL spectra of the corresponding compounds displayed in Figure 2. The similarity of the EL and PL spectra proves that the light is definitely emitted from the TPA-BT-containing molecules. The devices emit bright red light with the EL peak at ca. 620 nm and the Commission International de L'Eclairage (CIE) coordinates of the emitted light located at (0.61, 0.32).

Figure 6a displays the dependence of current density (I) and luminance (L) on voltage (V) ($I-V$ and $L-V$ curves) for the red-emitting devices. These devices exhibit relatively low turn-on voltages (corresponding to a brightness of 1 cd/m^2) at 2.0−2.5 V and high maximum luminance. In assessing the performance of these three devices, device A based on TPA-BT is the best, with the highest luminance of 12,192 cd/m^2 at 7.9 V and the maximum EL efficiency of 1.66 cd/A. The highest luminance of device B and device C is 8695 cd/m^2 at 9.2 V and 3142 cd/m^2 at 8.4 V, respectively. The maximum current efficiencies are 0.46 and 0.15 cd/A for device B and device C, respectively. The device performance of the three compounds is getting better with the decrease of the branches of the molecules. It is noteworthy that these devices all show reasonably stable efficiency over a broad current range, as shown in Figure 6b, which is a satisfactory performance meeting the need for active-matrix-driven devices.

TABLE 1: Photophysical Properties, Fluorescence Quantum Yields, and Optical Band Gaps of the Three Compounds

molecule	λ_{abs} (nm) (solution)	λ_{abs} (nm) (film)	λ_{em} (nm) (solution)	λ_{em} (nm) (film)	ϕ_{PL} [a]	E_g^{opt} [b]
TPA-BT	315, 490	317, 496	643	629	0.47	2.08
b-TPA-BT	326, 496	327, 504	643	631	0.54	2.06
t- TPA-BT	328, 501	327, 509	643	642	0.54	2.05

[a] The fluorescence quantum yields in toluene were obtained using DCM as the standard. [b] The optical band gap was obtained from the equation $E_g^{opt} = 1240/\lambda_{edge}$, where λ_{edge} is the onset value of the absorption spectrum in the long wavelength direction.

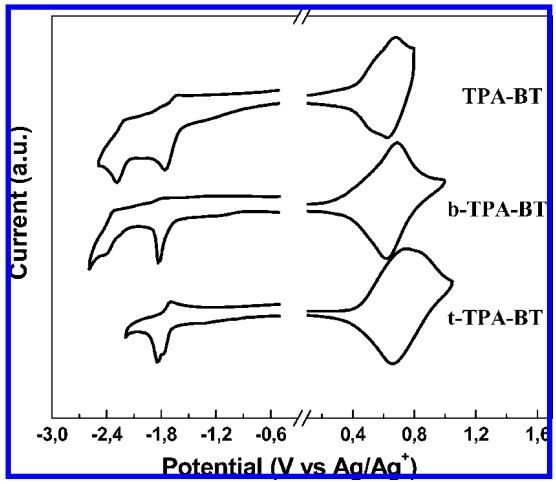

Figure 3. Cyclic voltammograms of TPA-BT, b-TPA-BT, and t-TPA-BT films on a platinum electrode in 0.1 mol/L Bu_4NPF_6, acetonitrile solution.

TABLE 2: Electrochemical Onset Potentials and Electronic Energy Levels

molecule	E_{ox}^{onset} (V)	E_{red}^{onset} (V)	HOMO (eV)	LUMO (eV)	E_g^{CV} (eV)
TPA-BT	0.43	−1.63	−5.14	−3.08	2.06
b-TPA-BT	0.36	−1.68	−5.07	−3.03	2.05
t-TPA-BT	0.44	−1.72	−5.15	−2.99	2.16

The EL performance of the OLED devices, PL peak wavelength of the corresponding compound films, and CIE coordinate of the EL emission are summarized in Table 3. Since the device performance could be partially affected by film morphology, we employed atomic force microscopy (AFM) to investigate the morphology difference among the three compounds films. To avoid the effect of experimental conditions, the films were fabricated under the same spin-coating conditions including speed, time, and solvent. As shown in Figure 7, TPA-BT film displays a smooth and featureless image over the 5 ×

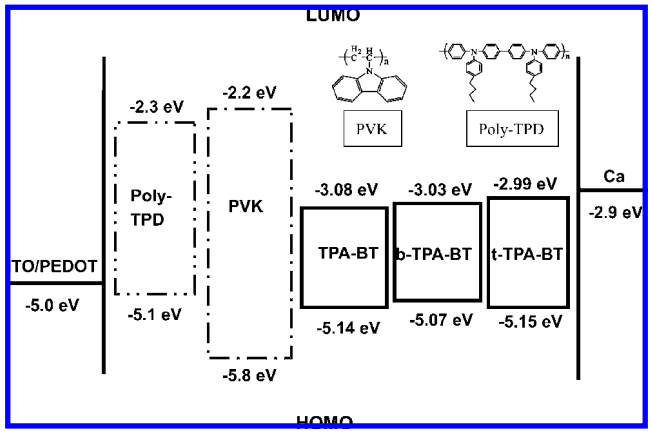

Figure 4. Energy-level diagram of the OLEDs.

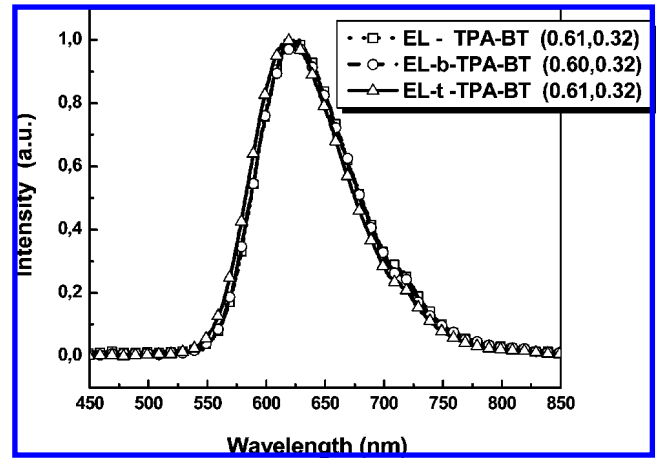

Figure 5. EL spectra and the CIE coordinates (shown in the brackets) of the OLEDs based on TPA-BT, b-TPA-BT, and t-TPA-BT.

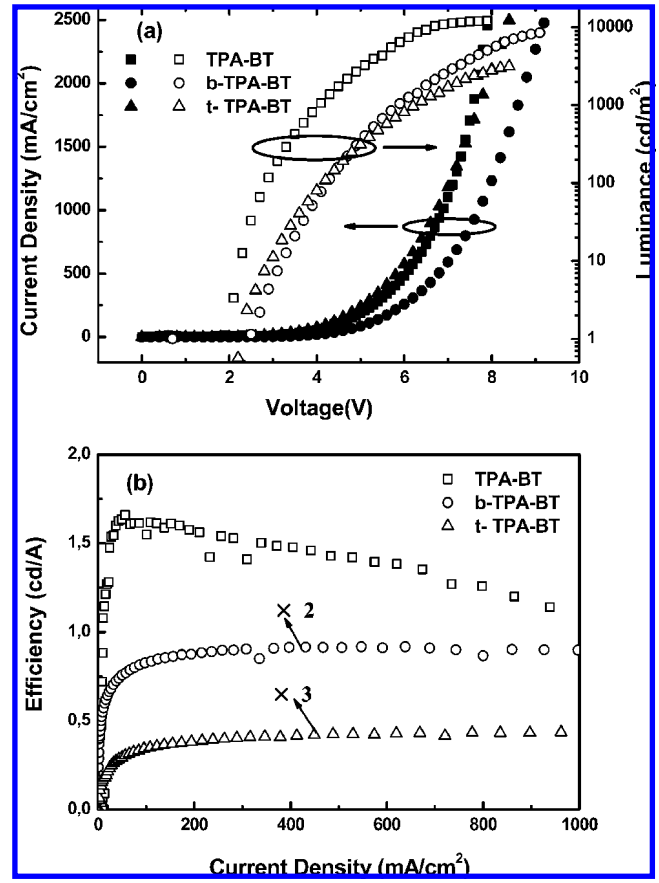

Figure 6. (a) Current−voltage and luminance−voltage characteristics and (b) current efficiency characteristics of the three OLED devices.

5 μm^2 scan area, suggesting a homogeneous morphology without any phase segregation. In contrast, the film formed by b-TPA-BT shows some nanoparticles in its AFM image, and lots of pinholes can be observed in the t-TPA-BT film. The morphology difference of the films could be the reason why the performance

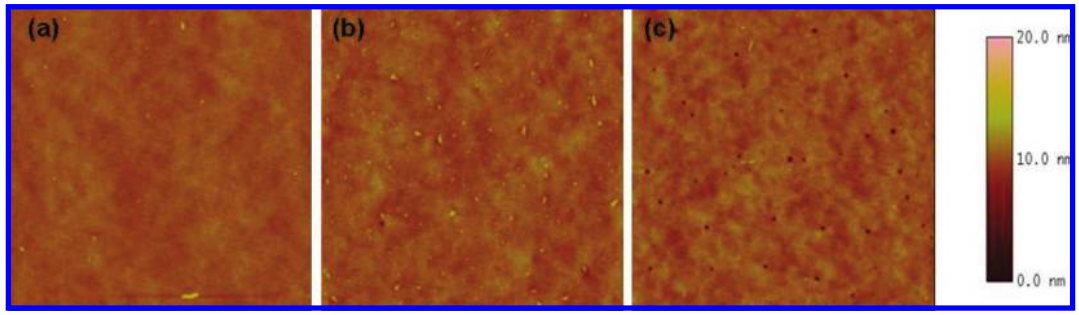

Figure 7. AFM images (5 μm × 5 μm) of (a) TPA-BT, (b) b-TPA-BT, and (C) t-TPA-BT films spin coated from toluene solutions.

of device B and device C is poorer than that of device A, since charge carrier leakage and/or charge trapping may occur at the rough films, resulting in lower luminance and EL efficiency.[48] The reason causing the morphology difference is still under investigation.

2.5. WLEDs Based on the Compounds as Red Emitters. On the basis of the red-emission characteristics of the TPA-BT-containing compounds mentioned above, white-light-emitting diodes (WLEDs) were fabricated by separately doping the three compounds as the red emitter and poly(6,6′-bi(9,9′-dihexylfluorene)-*co*-(9,9′-dihexylfluorene-3-thiophene-5′-yl)) (PFT) as green emitter into blue poly(9,9-dioctylfluorene-2,7-diyl) (PFO) host material. We employed two polyfluorene derivatives, PFO and PFT, as the blue- and green-light-emitting materials, respectively, in considering their good compatibility for reducing phase separation between them.[45] PFO was selected as the blue-light-emitting host polymer because of its high photoluminescence efficiency, good charge transport, and thermal stability. Moreover, due to the larger band gap of PFO, green and red light can be realized through an energy transfer and/or a charge trapping process from host PFO to guest molecules.[49,50] The structure of the three WLEDs is ITO/PEDOT:PSS(30 nm)/HTL(40 nm)/EML(60 nm)/Ca(10 nm)/Al(100 nm). The HTL is composed of the blend of PVK and poly-TPD (1:1, wt/wt) as that in the red OLEDs mentioned above, and the EML is the film of blue PFO host doped with green emitter PFT and red emitter TPA-BT, b-TPA-BT, or t-TPA-BT. Again, for the convenience of discussion, the devices containing TPA-BT, b-TPA-BT, and t-TPA-BT as red emitter were named as device D, device E, and device F, respectively. Since the color of the emitting light greatly depends on the ingredient ratio of the RGB components in the EML, we adjusted the weight ratios of the three components to obtain pure white light according to the EL spectra and the CIE coordinate values. The optimized ratios were PFO:PFT:TPA-BT = 1:0.035:0.007 for device D, PFO:PFT:b-TPA-BT = 1:0.04:0.0065 for device E, and PFO:PFT:t-TPA-BT = 1:0.035:0.006 for device F.

The EL spectra of the three devices are shown in Figure 8. It reveals that the emission band of the three devices covers the whole visible range from 380 to 780 nm. Blue emission at 430 nm was assigned to the emission of PFO. Green emission around 480 nm was from PFT. Also, the red emissions above 600 nm were from the TPA-BT-containing molecules. The inset

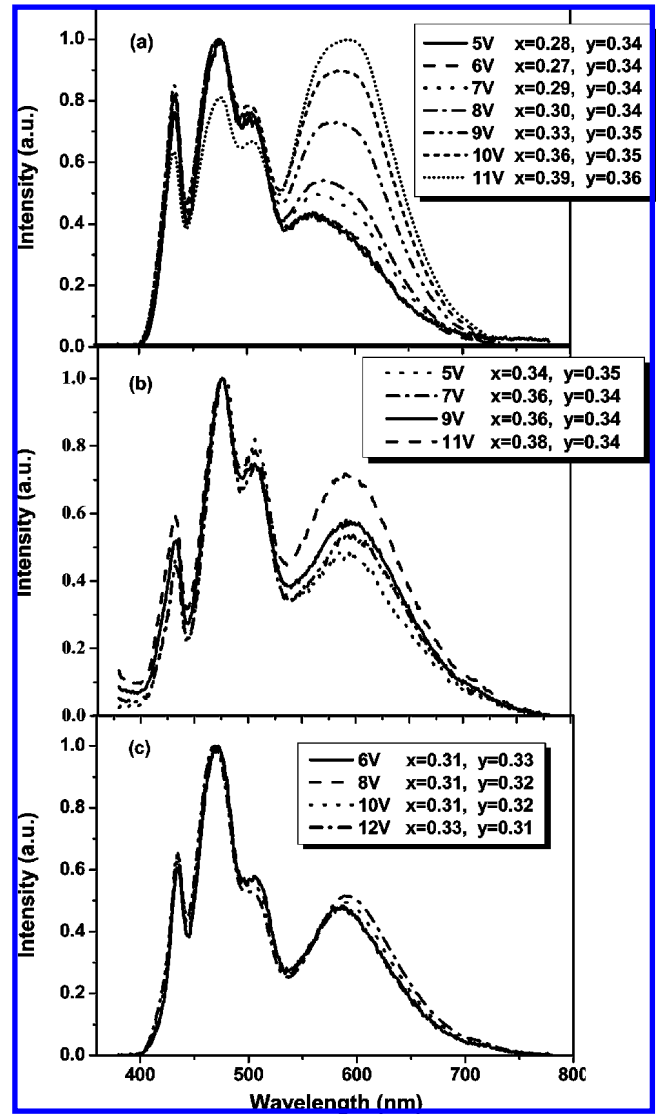

Figure 8. EL spectra and the CIE coordinates of the WLEDs: device D (a), device E (b), and device F (c) at different voltages.

of Figure 8 is the CIE coordinates of the white light emission from the devices at different voltages; they change slightly from (x = 0.28, y = 0.34) at 5.0 V to (x = 0.39, y = 0.36) at 11.0

TABLE 3: Luminance Characteristics of the OLEDs Based on s-TPA, d-TPA, and t-TPA

EML	turn-on voltage (V)	max luminance (cd/m^2) [at the voltage (V), current density (mA/cm^2)]	EL efficiency (cd/A) [at the voltage (V), current density (mA/cm^2)]	EL peak wavelength (nm)	PL peak wavelength of film (nm)	CIE coordinates
TPA-BT	2.0	12192 [7.9, 2456.1]	1.66 [4.0, 56.4]	620	629	(0.61, 0.32)
b-TPA-BT	2.5	8695 [9.2, 2479.4]	0.46 [6.6, 431.3]	620	631	(0.60, 0.32)
t- PA-BT	2.3	3142 [8.4, 2498.9]	0.15 [6.7, 962.1]	620	642	(0.61, 0.32)

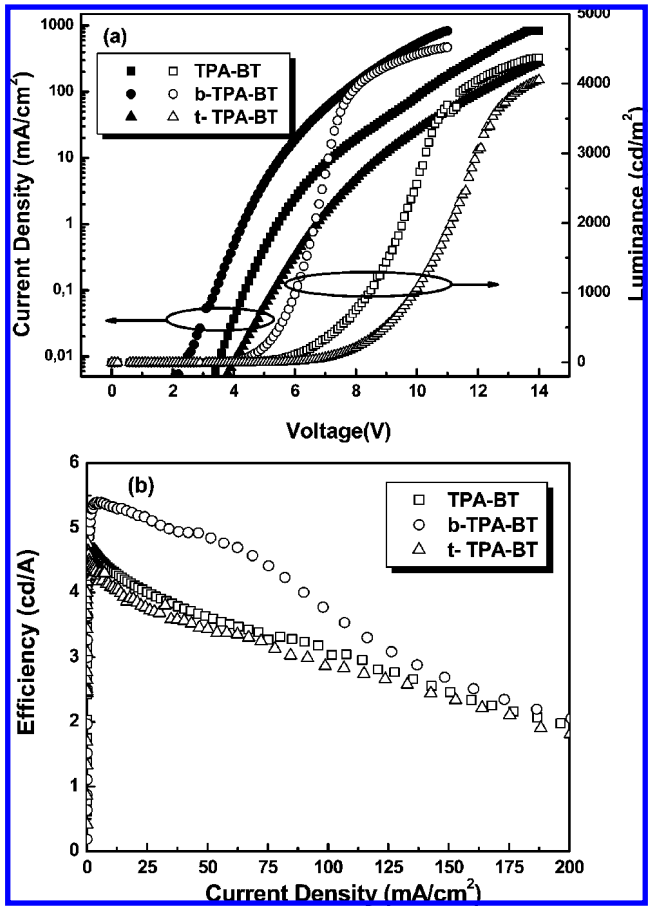

Figure 9. (a) Current−voltage and luminance−voltage characteristics and (b) current efficiency characteristics of the three WLEDs.

V for device D, from ($x = 0.34$, $y = 0.25$) at 5.0 V to ($x = 0.38$, $y = 0.34$) at 11.0 V for device E, and from ($x = 0.31$, $y = 0.33$) at 6.0 V to ($x = 0.33$, $y = 0.31$) at 12.0 V for device F. Within the above voltage ranges, the white light we obtained is stable and fairly close to the standard white light (CIE coordinate value of 0.33, 0.33). Furthermore, the color stability of the WLEDs with changing voltage is improved with the increase of the branches of red-emission compounds. For device F with the star-shaped t-TPA-BT as the red emitter, the CIE coordinates at different voltages were almost identical, which may be attributed to the special structure of the t-TPA-BT molecules. Probably, with the increase of the branches of the molecules, the distribution of the molecules in the host polymer film is more homogeneous and the morphology of the film is more uniform, so they stabilize the emitting color of the diodes.

Figure 9 shows the $I-V$ and $L-V$ curves of the WLED devices, and the performance of the WLEDs is summarized in Table 4. Low turn-on voltage and high-performance WLEDs were achieved with the TPA-BT-containing molecules as red emitter: the maximum luminance was around 4400 cd/m^2, and the maximum current efficiency reached above 4.5 cd/A. Compared to an earlier report,[51] the performances of these WLEDs have been greatly improved by using the binary host as the HTL. Being dissimilar from the red-light-emitting OLEDs, there were no obvious difference in the maximum luminance or luminescence efficiency among the three WLEDs, which may be attributed to the small doping amount of the red-light emitter in the WLEDs. In addition, the WLEDs are suitable for application in full-color displays with color filters, owing to its simultaneous red, green, and blue emission.

3. Conclusions

We designed and successfully synthesized a novel series of solution-processable red-emission organic molecules, TPA-BT, b-TPA-BT, and t-TPA-BT, with hole-transporting TPA as the core part and D−π−A push−pull structure as the branch part. High-performance red-emission OLEDs were fabricated with the compounds as the emissive layer using the spin-coating technique. Among the red OLEDs, the device based on TPA-BT displayed a maximum luminance of 12,192 cd/m^2 and a maximum current efficiency of 1.66 cd/A, which is among the highest values for the solution-processed red-emission OLEDs. Furthermore, WLEDs were fabricated by doping the molecules as red emitter and PFT as green emitter into blue PFO host polymer, and stable white light emission was realized with the maximum luminance around 4400 cd/m^2 and maximum efficiency above 4.5 cd/A. The results indicate that the three organic compounds reported in this paper are promising red-emitting organic materials for solution-processed light-emitting diodes.

4. Experimental Section

Materials. Poly(9,9-dioctylfluorene-2,7-diyl) (PFO) and poly(*N*,*N*′-bis(4-butylphenyl)-*N*,*N*′-bis(phenyl)benzidine) (poly-TPD) were purchased from American Dye Source, Inc., poly(*N*-vinylcarbazole) (PVK) was purchased from Aldrich Chemical Co., and they were used as received without any further purification. Poly(3,4-ethylene dioxythiophene):poly(styrene sulfonate) (PEDOT:PSS) was purchased from Bayer Co. (Germany).

Synthesis. ***Tris(4-(4,4,5,5-tetramethyl-1,3,2-dioxaborolan-2-yl)phenyl)amine (Compound 1).*** Tris(4-bromophenyl)amine (0.27 g, 1.45 mmol) was dissolved in 4 mL of THF; then it was cooled to −78 °C. *n*-BuLi (2.6 mmol) was added dropwise and kept at −78 °C for 1 h. 2-Isopropoxy-4,4,5,5-tetramethyl-1,3,2-dioxaborolane (2.43 mL, 13 mmol) was added dropwise. After addition, the reaction temperature was elevated to room temperature for overnight reaction. A 5 mL amount of H_2O was added for quenching the reaction. The water layer was extracted with methylene chloride; the organic layer was combined and dried over $MgSO_4$. After the volatile solvent was removed under reduced pressure, it was subjected to column separation (SiO_2, petroleum ether/ethyl acetate 1:1); 0.78 g of white solid with a yield of 83.9% was obtained.

^{1}H NMR 300 MHz (δ ppm): 7.66 (d, $J = 6.15$ Hz, 6 H), 7.06 (d, $J = 6.15$ Hz, 6 H), 1.33 (s, 36 H). MALDI-TOF MS: calcd for $C_{36}H_{48}B_3NO_6$, 623.38; found, 624.0

N-(4-(2-(4-Bromobenzo[c][1,2,5]thiadiazol-7-yl)vinyl)phenyl)-N-phenylbenzenamine (Compound 2). A mixture of *N*-phenyl-*N*-(4-vinylphenyl)benzenamine (1.5739 g, 5.8 mmol), 4,7-dibromobenzo[*c*][1,2,5]thiadiazole (1.705 g), $Pd(OAc)_2$ (26 mg, 2% molar amount), NaOAc (4.76 g, 58 mmol), and *n*-Bu_4NBr (0.30 g, 0.928 mmol) was dissolved in freshly distilled and degassed DMF (60 mL). The solution was kept at 100 °C for 24 h. A 100 mL amount of distilled water was added. The precipitate was filtered, washed with water, dissolved in methylene chloride, and dried over $MgSO_4$. After the solvent was evaporated under reduced pressure, it was subjected to column separation (SiO_2, petroleum ether/methane chloride 3:1). A 671 mg amount of compound **2** was obtained with a yield of 24%. ^{1}H NMR 300 MHz (δ ppm): 7.04 (m, $J = 8.66$, 8.0 Hz, 4 H), 7.12 (d, $J = 8.0$ Hz, 4 H), 7.28 (d, $J = 7.66$, 4 H), 7.44 (d, $J = 16.3$, 1 H), 7.49−7.53 (m, 3 H), 7.81 (d, $J = 7.5$ Hz, 1 H), 7.89 (d, $J = 16.3$ Hz, 1 H). ^{13}C NMR (δ ppm): 111.72, 121.69, 122.99 (×2), 123.36 (×2), 124.80 (×4), 126.11, 127.90 (×2), 129.34 (×5), 130.63, 130.90, 132.13, 133.77, 147.33 (×2),

TABLE 4: Optimized Blend Ratios in the Emissive Layer (EML) and the Corresponding Luminance Characteristics of the Three WLEDs

	blend weight ratios in EML B[a]:G[b]:R[c]	turn-on voltage (V)	EL efficiency (cd/A) [at the voltage (V), current density (mA/cm^2)]	max luminance (cd/m^2) [at the voltage (V), current density (mA/cm^2)]	CIE coordinates [at the voltage (V), current density (mA/cm^2)]
device D	1:3.5%:0.7%	3.1	4.76 [4.9, 16.5]	4366 [14.0, 833.3]	(0.33, 0.35) [9.0, 40.3]
device E	1:4%:0.65%	3.3	5.39 [5.2, 5.9]	4524 [11.0, 833.3]	(0.36, 0.34) [7.0, 56.8]
device F	1:3.5%:0.6%	4.1	4.69 [6.9, 60.3]	4341 [16.9, 794.7]	(0.31, 0.32) [10, 26.7]

[a] Blue emitter: PFO. [b] Green emitter: PFT. [c] Red emitter: TPA-BT for device D, b-TPA-BT for device E, and t-TPA-BT for device F.

148.17, 152.96, 153.83. MALDI-TOF MS: calcd for $C_{26}H_{18}BrN_3S$, 483.04; found, 483.4

4-(4-(4-(Diphenylamino)styryl)benzo[c][1,2,5]thiadiazol-7-yl)-N-(4-(4-(4-(diphenylamino)styryl)benzo[c][1,2,5]thiadiazol-7-yl)phenyl)-N-phenylbenzenamine (b-TPA-BT) and Tris(4-(4-(4-(diphenylamino)styryl)benzo[c][1,2,5]thiadiazol-7-yl)phenyl)amine (t-TPA-BT). To a mixture of compound **1** (0.148 g, 0.238 mmol), compound **2** (0.38 g, 0.786 mmol), $Pd(PPh_3)_4$ (41 mg, 1.5% molar amount), K_2CO_3 (0.493 g, 3.57 mmol), *n*-Bu_4NBr (0.253 g, 0.786 mmol), toluene (10 mL), and water (3.0 mL) were injected by syringe. The reaction mixture was heated to 100 °C and kept for 24 h. The reaction was quenched by addition of 1 N HCl. The water layer was extracted with methylene chloride and dried over $MgSO_4$. Volatile solvent was removed under reduced pressure. Then it was separated by column ((SiO_2, petroleum ether/methane chloride 4:1). A 55 mg amount of b-TPA-BT was collected with a yield of 22%. A 125 mg amount of t-TPA-BT corresponds to a yield of 36%.

b-TPA-BT. ^{1}H NMR 400 MHz (δ ppm): 7.04−7.10 (m, 8 H), 7.13 (d, J = 8.1 Hz, 9 H), 7.28−7.34 (m, 16 H), 7.53 (d, J = 8.4 Hz, 4 H), 7.56 (d, J = 16.4 Hz, 2 H), 7.71−7.74 (d, d, J =, 4 H), 7.91 (d, J = 8.3 Hz, 4 H), 7.92 (d, J = 16.4 Hz, 2 H). ^{13}C NMR: 122.62, 123.21 (×3), 123.24 (×3), 123.69 (×2), 123.82, 124.68, 125.47, 126.31, 127.47, 127.80 (×2), 129.31 (×8), 129.45, 129.49, 129.96 (×2), 131.49, 131.66, 131.80, 132.56, 147.13, 147.44 (×2), 147.54, 147.84, 154.00, 154.08. MALDI-TOF MS: calcd for $C_{70}H_{49}N_7S_2$, 1051.35; found, 1051.8. Anal. Calcd for $C_{70}H_{49}N_7S_2$: C, 79.90; H, 4.69; N, 9.32; S, 6.09. Found: C, 79.78; H, 4.78; N, 9.20; S, 6.24.

t-TPA-BT. ^{1}H NMR (δ ppm): 7.06−7.10 (m, 12 H), 7.13 (d, J = 8.0 Hz, 12 H), 7.28 (d, J = 7.8 Hz, 12 H), 7.40 (d, J = 8.5 Hz, 6 H), 7.53 (d, J = 6.24 Hz, 6 H), 7.60 (d, J = 16.4 Hz, 3 H), 7.73 (quar, 6 H), 7.93 (d, J = 16.4 Hz, 3 H), 7.97 (d, J = 8.5 Hz, 6 H). ^{13}C NMR: 122.58, 123.22 (×4), 124.35, 124.69 (×4), 126.28, 127.54, 127.82 (×2), 129.32, 129.53 (×6), 130.10, 131.46, 131.65, 132.20, 132.60, 147.17, 147.43 (×2), 147.85, 153.96, 154.06. MALDI-TOF MS: calcd for $C_{96}H_{66}N_{10}S_3$, 1454.46; found, 1454.9. Anal. Calcd for $C_{96}H_{66}N_{10}S_3$: C, 79.20; H, 4.57; N, 9.62; S, 6.61. Found: C, 79.06; H, 4.69; N, 9.70; S, 6.54.

TPA-BT. TPA-BT was synthesized based on the same method as b-TPA-BT via coupling reaction of *N*-(4-(1,5-dimethyl-2,4-dioxa-3-bora-bicyclo[3.1.0]hexan-3-yl)phenyl)-*N*-phenylbenzenamine and compound **2.** A red solid with a yield of 97% was obtained. ^{1}H NMR (δ ppm): 7.04−7.10 (m, 6 H), 7.13 (d, J = 7.9 Hz, 4 H), 7.18−7.21 (m, 6 H), 7.28 (m, 8 H), 7.52 (d, J = 8.0 Hz, 2 H), 7.55 (d, J = 16 Hz, 1 H), 7.67 (d, J = 7.4 Hz, 1 H), 7.72 (d, J = 7.4 Hz, 1 H), 7.87 (d, J = 8.0 Hz, 2 H), 7.91 (d, J = 16 Hz, 1 H). MALDI-TOF MS: calculated for $C_{44}H_{32}N_4S$ 648.23, found 648.2. Anal. Calcd for $C_{44}H_{32}N_4S$: C, 81.45; H, 4.97; N, 8.64; S, 4.94. Found: C, 81.52; H, 4.89; N, 8.73; S, 4.84. The melting points of the three compounds are 224, 130, and 141 °C for TPA-BT, b-TPA-BT, and t-TPA-BT, respectively.

Physical Measurements. All new compounds were characterized by ^{1}H NMR taken on a Bruker DMX-400 spectrometer. For the ^{1}H NMR measurements, $CDCl_3$ was used as the solvent. Chemical shifts of NMR were reported in ppm relative to the singlet as 7.26 ppm for ^{1}H NMR. Photoluminescence (PL) and electroluminescence (EL) spectra were recorded with a Hitachi F-4500 fluorescence spectrophotometer. The highest occupied molecular orbital (HOMO) and the lowest unoccupied molecular orbital (LUMO) energy levels of the polymers used in this work were calculated from the onset oxidation and onset reduction potentials measured by cyclic voltammetry (CV). The CV measurement was performed on a Zahner IM6e electrochemical workstation, using molecules films on Pt disk as the working electrode, Pt wire as the counter electrode, and Ag/Ag^+ as the reference electrode, in a 0.1 M tetrabutylammonium hexafluorophosphate acetonitrile solution. All measurements were performed under an ambient atmosphere at room temperature.

Device Fabrication and Characterization. The device configuration is ITO/PEDOT:PSS(30 nm)/HTL(40 nm)/EML(60 nm)/Ca(10 nm)/Al(100 nm). The fabrication process of the device is as follows. The ITO-coated glass substrate was first cleaned with detergent, then ultrasonicated in acetone and isopropyl alcohol, and subsequently dried in an oven. Then PEDOT:PSS (Baytron PVP AI 4083 Germany) was spin cast (2000 rpm) with a thickness of ~30 nm from aqueous solution (after passing through a 0.45 μm filter). The substrate was dried at 150 °C for 30 min in air and then moved into a glovebox for spin casting the active layers. Third, the binary-host PVK/poly-TPD were dissolved in chlorobenzene and spin cast on top of the PEDOT:PSS as the HTL (host-transporting layer). The HTL was treated by annealing at 110 °C for 45 min. Then, the solution of the light-emitting materials in toluene was spin cast on the top of the HTL as the EML. Similarly, the EML was also treated by thermal annealing at 100 °C for 30 min. Last, a layer of Ca capped with Al was thermally deposited through a shade mask at a pressure of ca. 5×10^{-5} Pa. The thickness of the active layer was determined by an Ambios Tech. XP-2 profilometer. The current−voltage ($I-V$) and luminance−voltage ($L-V$) characteristics were conducted on a computer-controlled Keithley 236 Source-Measure Unit and a Keithley 2000 Multimeter coupled with a Si photomultiplier tube.

Acknowledgment. This work was supported by the NSFC (nos. 50633050, 20721061, and 20773156).

References and Notes

(1) Tang, C. W.; VanSlyke, S. A. *Appl. Phys. Lett.* **1987**, *51*, 913.
(2) Burroughes, J. H.; Bradley, D. D. C.; Brown, A. R.; Marks, R. N.; Mackay, K.; Friend, R. H.; Burns, P. L.; Holmes, A. B. *Nature* **1990**, 539.
(3) Sheats, J. R.; Antoniadis, H.; Hueschen, M.; Leonard, W.; Miller, J.; Moon, R.; Roitman, D.; Stocking, A. *Science* **1996**, *273*, 884.
(4) Gross, M.; Muller, D. C.; Nothofer, H. Z.; Scherf, U.; Neher, D.; Bräuchle, C.; Meerholz, K. *Nature* **2000**, *405*, 661.
(5) (a) Shirota, Y.; Kageyama, H. *Chem. Rev.* **2007**, *107*, 953. (b) Tang, R. P.; Tan, Z. A.; Li, Y. F.; Xi, F. *Chem. Mater.* **2006**, *18*, 1053.
(6) Hung, L. S.; Chen, C. H. *Mater. Sci. Eng. Rev* **2002**, *39*, 143.
(7) Fuhrmann, T.; Salbeck, J. *MRS Bull.* **2003**, *28* (5), 354.
(8) Wu, W. C.; Yeh, H. C.; Chan, L. H.; Chen, C. T. *Adv. Mater.* **2002**, *14*, 1072.

(9) Thomas, K. R. J.; Lin, J. T.; Tao, Y. T.; Chuen, C. H. *Adv. Mater.* **2002**, *14*, 822–826.
(10) Chen, C. H.; Shi, J.; Tang, C. W. *Macromol. Symp.* **1998**, *125*, 1.
(11) Ma, C. Q.; Liang, Z.; Wang, X. S.; Zhang, B. W.; Cao, Y.; Wang, L. D.; Qiu, Y. *Synth. Met.* **2003**, *138*, 537.
(12) Tang, C. W.; VanSlyke, S. A.; Chen, C. H. *J. Appl. Phys.* **1989**, *65*, 3610.
(13) Chen, C. H.; Shi, J.; Tang, C. W. *Macromol. Symp.* **1997**, *125*, 1.
(14) Chen, C. H.; Tang, C. W.; Shi, J.; Klubek, K. P. *Thin Solid Films* **2000**, *363*, 327.
(15) Burrows, P. E.; Forrest, S. R.; Sibley, S. P.; Thompson, M. E. *Appl. Phys. Lett.* **1996**, *69*, 2959.
(16) Morgado, J.; Cacialli, F.; Iqbal, R.; Moratti, S. C.; Holmes, A. B.; Yahioglu, G.; Milgrom, L. R.; Friend, R. H. *J. Mater. Chem.* **2001**, *11*, 278.
(17) Sakakibara, Y.; Okutsu, S.; Enokida, T.; Tani, T. *Appl. Phys. Lett.* **1999**, *74*, 2588.
(18) Chen, C. T. *Chem. Mater.* **2004**, *16*, 4389. (b) He, Q. G.; Lin, T.; Bai, F. L. *Chin. Sci. Bull.* **2000**, *45*, 2376.
(19) Hamada, Y.; Kanno, H.; Tsujioka, T.; Takahashi, H.; Usuki, T. *Appl. Phys. Lett.* **1999**, *75*, 1682.
(20) Kinoshita, M.; Fujii, N.; Tsuzuki, T.; Shirota, Y. *Synth. Met.* **2001**, *121*, 1571.
(21) Doi, H.; Kinoshita, M.; Okumoto, K.; Shirota, Y. *Chem. Mater.* **2003**, *15*, 1080.
(22) Shirota, Y.; Kinoshita, M.; Noda, T.; Okumoto, K.; Ohara, T. *J. Am. Chem. Soc.* **2000**, *122*, 11021.
(23) Maede, M.; Hashimoto, K.; Okumoto, K.; Shirota, Y. *Polym. Prepr. Jpn.* **2004**, *53*, 2–4559.
(24) He, C.; He, Q. G.; Yi, Y. P.; Wu, G. L.; Bai, F. L.; Shuai, Z. G.; Li, Y. F. *J. Mater. Chem.* **2008**, *18*, 4085.
(25) Adachi, C.; Tsutsui, T.; Saito, S. *Appl. Phys. Lett.* **1990**, *56*, 799.
(26) He, Q. G.; Lin, H. Z.; Weng, Y. F.; Zhang, B.; Wang, Z. M.; Lei, G. T.; Wang, L. D.; Qiu, Y.; Bai, F. L. *Adv. Funct. Mater.* **2006**, *16*, 1343.
(27) Thomas, K. R. J.; Lin, J. T.; Velusamy, M.; Tao, Y. T.; Chuen, C. H. *Adv. Funct. Mater.* **2004**, *14*, 83.
(28) Fang, Q.; Xu, B.; Jiang, B.; Fu, H. T.; Chen, X. Y.; Cao, A. *Chem. Commun.* **2005**, 1468.
(29) Akhtaruzzaman, M.; Tomura, M.; Zaman, M. B.; Nishida, J.; Yamashita, Y. *J. Org. Chem.* **2002**, *67*, 7813.
(30) Shi, C. J.; Wu, Y.; Zeng, W. J.; Xie, Y. Q.; Yang, K. X.; Cao, Y. *Macromol. Chem. Phys.* **2005**, *206*, 1114.
(31) Brabec, C. J.; Winder, C.; Sariciftci, N. S.; Hummelen, J. C.; Dhanabalan, A.; van Hal, P. A.; Janssen, R. A. J. *Adv. Funct. Mater.* **2002**, *12*, 709.
(32) Wu, I. Y.; Lin, J. T.; Tao, Y. T.; Balasubramaniam, E.; Su, Y. Z.; Ko, C. W. *Chem. Mater.* **2001**, *13*, 2626.
(33) Katsuma, K.; Shirota, Y. *Adv. Mater.* **1998**, *10*, 223.
(34) Shirota, Y. *J. Mater. Chem.* **2005**, *15*, 75.
(35) Cravino, A.; Leriche, P.; Aleveque, O.; Roquet, S.; Roncali, J. *Adv. Mater.* **2006**, *18*, 3033.
(36) Lee, Y. T.; Chiang, C. L.; Chen, C. T. *Chem. Commun.* **2008**, 217.
(37) Liu, J.; Chen, L.; Shao, S. Y.; Xie, Z. Y.; Cheng, Y. X.; Geng, Y. H.; Wang, L. X.; Jing, X. B.; Wang, F. S. *J. Mater. Chem.* **2008**, *18*, 319.
(38) Roquet, S.; Cravino, A.; Leriche, P.; Aleveque, O.; Frere, P.; Roncali, J. *J. Am. Chem. Soc.* **2006**, *128*, 3459.
(39) Zhou, Y.; He, Q. G.; Yang, Y.; Zhong, H. Z.; He, C.; Sang, G. Y.; Liu, W.; Yang, C. H.; Bai, F. L.; Li, Y. F. *Adv. Funct. Mater.* **2008**, *18*, 3299.
(40) Jayakannan, M.; Van Hal, P. A.; Janssen, R. A. J. *J. Polym. Sci., Part A: Polym. Chem.* **2002**, *40*, 2360.
(41) Jayakannan, M.; Van Hal, P. A.; Janssen, R. A. J. *J. Polym. Sci., Part A: Polym. Chem.* **2002**, *40*, 251.
(42) Raimundo, J. M.; Blanchard, P.; Brisset, H.; Akoudad, S.; Roncali, J. *Chem. Commun.* **2000**, 939.
(43) Karikomi, M.; Kitamura, C.; Tanaka, S.; Yamashita, Y. *J. Am. Chem. Soc.* **1995**, *117*, 6791.
(44) Sun, Q. J.; Wang, H. Q.; Yang, C. H.; Li, Y. F. *J. Mater. Chem.* **2003**, *13*, 800.
(45) Zhou, Y.; Sun, Q. J.; Tan, Z.; Zhong, H. Z.; Yang, C. H.; Li, Y. F. *J. Phys. Chem. C* **2007**, *111*, 6862.
(46) Sun, Q. J.; Hou, J. H.; Yang, C. H.; Li, Y. F.; Yang, Y. *Appl. Phys. Lett.* **2006**, *89*, 153501.
(47) Sun, Q. J.; Fan, B. H.; Tan, Z. A.; Yang, C. H.; Li, Y. F.; Yang, Y. *Appl. Phys. Lett.* **2006**, *88*, 163510.
(48) Ma, B.; Kim, B. J.; Deng, L.; Poulsen, D. A.; Thompson, M. E.; Frechet, J. M. J. *Macromolecules* **2007**, *40*, 8156.
(49) Miteva, T.; Meisel, A.; Knoll, W.; Nothofer, H. G.; Scherf, U.; Muller, D. C.; Meerholz, K.; Yasuda, A.; Neher, D. *Adv. Mater.* **2001**, *13*, 565.
(50) Scherf, U.; List, E. J. W. *Adv. Mater.* **2002**, *14*, 477.
(51) Bai, F. L.; He, Q. G.; Liu, W.; Zhou, Y.; Sun, Q. J.; Li, Y. F. *SPIE* **2007**, 6828–68280A.

JP900362F